Compressed sensing MRI with singular value decomposition-based sparsity basis



2011 Phys. Med. Biol. 56 6311

(http://iopscience.iop.org/0031-9155/56/19/010)

IOP PUBLISHING PHYSICS IN MEDICINE AND BIOLOGY

Phys. Med. Biol. **56** (2011) 6311–6325 doi:10.1088/0031-9155/56/19/010

# Compressed sensing MRI with singular value decomposition-based sparsity basis

**Mingjian Hong[1], Yeyang Yu[2], Hua Wang[2], Feng Liu[2,3] and Stuart Crozier[2]**

[1] School of Software Engineering, ChongQing University, ChongQing 400030, People's Republic of China
[2] School of Information Technology and Electrical Engineering, The University of Queensland, St Lucia, QLD 4072, Australia

E-mail: hmj@cqu.edu.cn, feng@itee.uq.edu.au, Yeyang.yu@uq.edu.au, hwang@itee.uq.edu.au and stuart@itee.uq.edu.au

Received 17 February 2011, in final form 3 August 2011
Published 6 September 2011
Online at stacks.iop.org/PMB/56/6311

**Abstract**

Compressed sensing MRI (CS-MRI) aims to significantly reduce the measurements required for image reconstruction in order to accelerate the overall imaging speed. The sparsity of the MR images in transformation bases is one of the fundamental criteria for CS-MRI performance. Sparser representations can require fewer samples necessary for a successful reconstruction or achieve better reconstruction quality with a given number of samples. Generally, there are two kinds of 'sparsifying' transforms: predefined transforms and data-adaptive transforms. The predefined transforms, such as the discrete cosine transform, discrete wavelet transform and identity transform have usually been used to provide sufficiently sparse representations for limited types of MR images, in view of their isolation to the object images. In this paper, we present singular value decomposition (SVD) as the data-adaptive 'sparsity' basis, which can sparsify a broader range of MR images and perform effective image reconstruction. The performance of this method was evaluated for MR images with varying content (for example, brain images, angiograms, etc), in terms of image quality, reconstruction time, sparsity and data fidelity. Comparison with other commonly used sparsifying transforms shows that the proposed method can significantly accelerate the reconstruction process and still achieve better image quality, providing a simple and effective alternative solution in the CS-MRI framework.

(Some figures in this article are in colour only in the electronic version)

[3] Author to whom any correspondence should be addressed.

  

## Introduction

Imaging speed in conventional magnetic resonance imaging (MRI) is limited by slow acquisition of full *k*-space using magnetic field gradients (Westbrook *et al* 2005). Traditional methods reduce the acquisition time of MRI using fast switching rates of gradients and RF pulses. Recently proposed fast imaging techniques can be generally categorized into three classes: parallel MRI (pMRI) (Larkman and Nunes 2007), compressed sensing MRI (CS-MRI) (Lustig *et al* 2007) and a combination of these two methods (Liang *et al* 2009, Otazo *et al* 2010). pMRI techniques explore information redundancies from multichannel coils to reconstruct object images based on spatial sensitivity inherence in the coils, such as SMASH (Sodickson and Manning 1997), SENSE (Pruessmann *et al* 1999), PILS (Griswold *et al* 2000) and GRAPPA (Griswold *et al* 2002), etc. Because of practical limitations such as the noise with resonant signal and the imperfect coil geometry, these techniques eventually force a trade-off between image quality and speed.

Based on CS theory (Donoho 2006), which relaxes the data measurement requirement that is essential to Nyquist–Shannon sampling theorem, CS-MRI exploits the sparsity of the signal itself to reconstruct the MR images from far fewer samples than conventional methods require, thus significantly reducing the scan time. CS-MRI generally solves an underdetermined system, while pMRI techniques seek solutions from redundant information in multiple channel coils, as an overdetermined problem. In the CS-MRI, the acceleration can be achieved with two fundamental conditions: (a) the object MR image should be sparse in a basis, and (b) the sensing matrix (Fourier encoding herein) should be incoherent with the sparsity basis. With these two conditions, we can accurately reconstruct the object image with appropriate nonlinear recovery algorithms. The nonlinear recovery systems are solved by minimizing the $l_1$ norm of the sparsified image, subject to the data fidelity constraint of the measurements. To ensure the second condition, which is the incoherence between the sensing matrix and the sparsity basis, a pseudo-random variable density *k*-space undersampling is normally applied. To ensure the first condition, which is the sparsity of the MR images, various sparsity bases have been applied. There are two broad types of sparsity bases: predefined bases and data-adaptive bases. The most commonly used sparsity bases are predefined, such as the bases of the discrete cosine transform (Ahmed *et al* 1974) and the wavelet transform (Mallat 1999). The transformation with these bases is isolated from the object image. Thus, some images show sufficient sparsity with these bases, while the others do not. In other words, one certain basis can only provide a sparse representation with limited kinds of object images. For instance, MR angiograms are usually sparse in the pixel domain, which leads to the identity transform as an ideal sparsifying transform. However, for more complex objects, such as brain images, the identity transform cannot provide a sufficiently sparse representation. Consequently, it is valuable to develop a data-adaptive sparsity basis, which can 'understand' what it is transforming and be trained from the object image samples, so that it can intrinsically provide a sufficiently sparse representation for a variety of images. For example, Bilgin *et al* 2010 used the K-SVD (Rubinstein *et al* 2010) algorithm to design data-adaptive sparsifying transform to reconstruct a restricted class of MR images. One of the most used data-adaptive transforms is the principal component analysis (PCA) (Jolliffe 2002). The PCA method constructs the data-adaptive basis through the calculation of eigenvectors of the sample covariance matrix consisting of many pre-scanned images. However, the dimension of the sample covariance matrix is usually excessively high, for example, 262 144 for $512 \times 512$ images, which requires intensive computation for the determination of the eigenvectors. To overcome this problem of PCA, a straightforward data projection technique, named 2D-PCA, was proposed (Yang *et al* 2004). The 2D-PCA relaxes the high-dimensional limitation by constructing the basis

directly from the image matrices. However, 2D-PCA still requires many prescanned images as in PCA, which is time consuming in the MRI scenario and therefore difficult to use.

To fulfill the practicability of using a data-adaptive sparsity basis in CS-MRI, in this work, we propose a method using SVD as a data-adaptive transform which requires no prescanned images as in PCA or 2D-PCA. This approach can potentially sparsify a greater variety of MR images than the predefined transforms, and still be efficient in the CS-MRI framework. Four different sparsifying transforms: discrete cosine transform (DCT), discrete wavelet transform (DWT), identity transform (IDT) and the proposed one are applied to MR brain image and angiogram, which represent typical MR images with diverse features, using different reduction factors to evaluate the performance in terms of the image quality, reconstruction time, sparsity and data fidelity.

## Methodology

### *Compressed sensing MRI (CS-MRI)*

The CS-MRI can be described mathematically as follows. Suppose $m$, which is known in advance to have a sparse representation in some basis $\psi$, is an $N \times N$ object MR image, and we can randomly obtain measurements from $k$-space data of this image. Then, the CS-MRI reconstruction model can be described as the following constrained optimization problem:

$$\begin{aligned} &\text{Minimize}: \ \|\psi(m)\|_0 \\ &\text{s.t.}, \quad \|\varphi_F(m) - y\|_2 < \varepsilon \end{aligned} \tag{1}$$

where $\psi$ denotes the sparsifying transform, $\varphi_F$ denotes the partial Fourier transform, $y$ is the measurements gathered from the MRI scanner, $\varepsilon$ relates to the noise level of the measurements. Because this problem was proved to be NP-hard (Candes *et al* 2006), the $l_0$ norm is replaced with the $l_1$ norm to enforce the sparsity and obtain a problem of convex optimization, which can be solved efficiently, as follows:

$$\begin{aligned} &\text{Minimize}: \quad \|\psi(m)\|_1 \\ &\text{s.t.}, \quad \|\varphi_F(m) - y\|_2 < \varepsilon. \end{aligned} \tag{2}$$

### *Constructing the sparsifying transform*

Sparsity plays a key role in how well we can estimate the object images, because it reduces the complexity of the image representation and permits the efficient compression of the object images. We can classify various sparsity bases into two categories, predefined bases and data-adaptive bases. Up until now, the most frequently used bases in the CS-MRI framework are predefined, such as the bases of the DCT, DWT and identity transform. However, one shortcoming of these kinds of bases is that they can only accurately represent a limited range of images or image features. In this work, we aim to construct a data-adaptive sparsifying transform, which can sparsify different kinds of MR images.

We made the observation that the image $\mathbf{I}_{zf}$ reconstructed by the direct inverse Fourier transform from the undersampled $k$-space is usually a good initial estimate of the target, because the centre of the $k$-space, which contains the dominant information of the target image, is still heavily sampled. If we can find a basis to sparsely represent $\mathbf{I}_{zf}$, then the target image should have a sparse representation in the same basis. This concept is shown in figure 1.

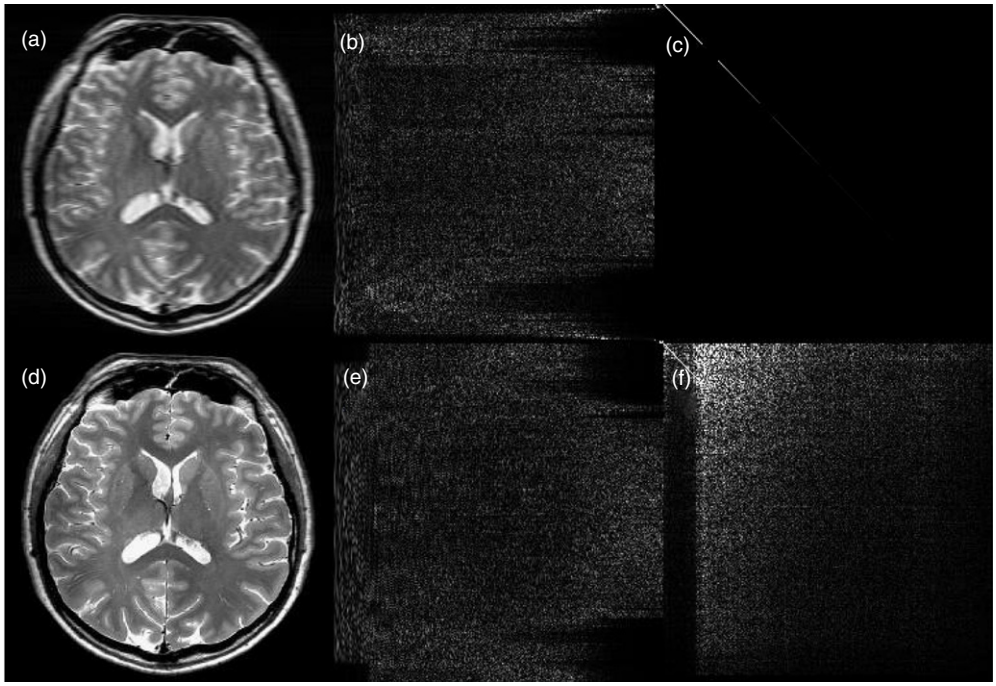


**Figure 1.** (a) $\mathbf{I}_{zf}$ by applying inverse Fourier transform to the randomly under-sampled $k$-space data; (b) the unitary matrix $\mathbf{U}$ obtained by performing SVD on $\mathbf{I}_{zf}$; (c) the diagonal matrix $\Sigma_{zf}$ of SVD on $\mathbf{I}_{zf}$; (d) the target image $\mathbf{I}_{\text{raw}}$; (e) the unitary matrix $\mathbf{V}$ of SVD on $\mathbf{I}_{zf}$; (f) the sparsified representation of the target image $\mathbf{I}_{\text{raw}}$.

The SVD is an important factorization scheme for a rectangular matrix. It is well known that SVD may be used to compress various data using reduced rank approximations. For image $\mathbf{I}_{zf}$, its SVD

$$\mathbf{I}_{zf} = \mathbf{U}\Sigma_{zf}\mathbf{V}^* \tag{3}$$

where $\mathbf{U}$ (figure 1(b)) and $\mathbf{V}$ (figure 1(e)) are two unitary matrices and $\Sigma_{zf}$ is a diagonal matrix $diag(\sigma_1, \sigma_2, \ldots, \sigma_r, 0, \ldots, 0)$ with $\sigma_1 \geqslant \sigma_2 \geqslant \sigma_r > 0$ (figure 1(c)), which is a very sparse representation of $\mathbf{I}_{zf}$. As is shown in figure 2, by using $\mathbf{I}_{zf} = \sum_{i=1}^{r} \sigma_i \mathbf{u}_i \mathbf{v}_i^T$, the image matrix $\mathbf{I}_{zf}$ can be approximated by discarding some outer products with small singular values. That is,

$$\mathbf{I}_{zf} \approx \mathbf{I}_{zf}^{(k)} = \sum_{i=1}^{k} \sigma_i \mathbf{u}_i \mathbf{v}_i^T, \quad k \leqslant r.$$

With this idea, the sparsifying transform can be derived as follows. $\mathbf{I}_{zf}$ (figure 1(a)) is reconstructed directly by the inverse Fourier transform from randomly undersampled $k$-space data with incoherent aliasing. The SVD is performed on $\mathbf{I}_{zf}$; we then derive the initial estimate of the sparsifying transform and its inverse with $\mathbf{U}$ and $\mathbf{V}$ as follows:

$$\begin{aligned} \Psi(m) &= \mathbf{U}m\mathbf{V}^* \\ \Psi^{-1}(x) &= \mathbf{U}^* x \mathbf{V}. \end{aligned} \tag{4}$$

Together with the equation (2), the problem of the CS-MRI with the SVD-based sparsifying transform is defined. From equations (2) and (4), the convex optimization algorithm can reconstruct an image better than $\mathbf{I}_{zf}$.

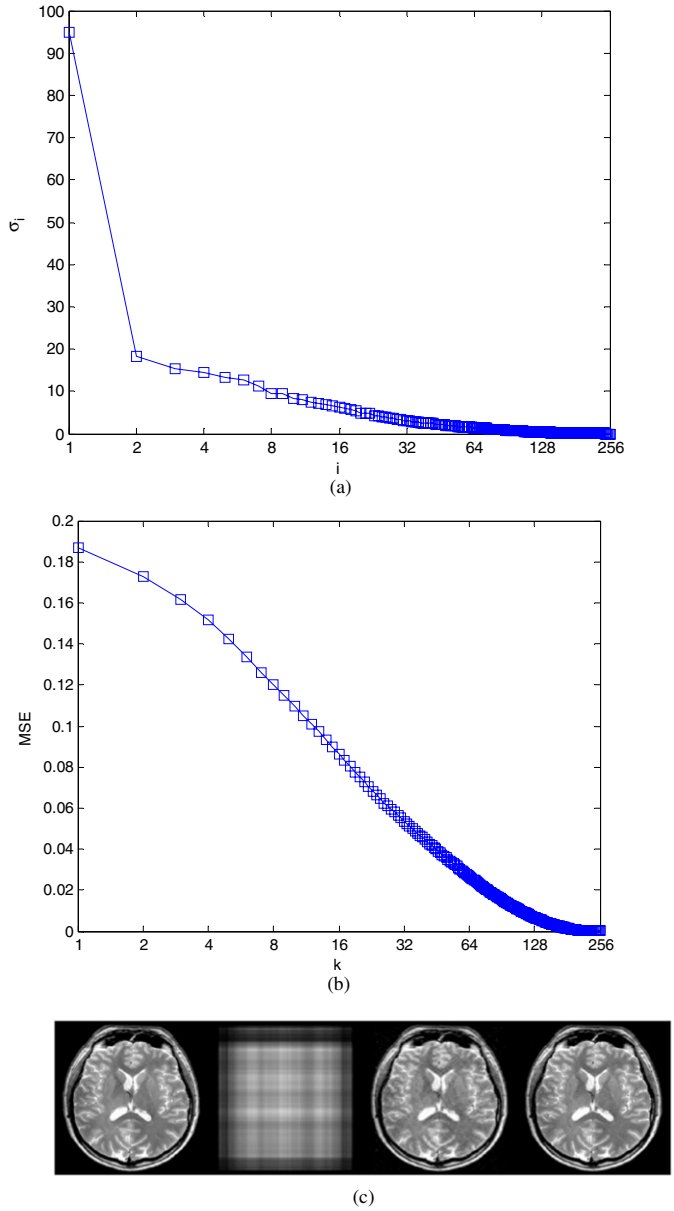


**Figure 2.** (a) The singular value $\sigma_i$; (b) the mean square error of the $\mathbf{I}_{zf}^{(k)}$; (c) from left to right: full image, $\mathbf{I}_{zf}^{(k)}$ with $k = 1, 40, 80$.

Because $\mathbf{I}_{zf}$ is an aliased version of the object image, the $\mathbf{U}$ and $\mathbf{V}$ in the equation (4) are not the optimal estimate of the sparsifying transform for the object image. To obtain a more sparse representation of the object image, we update the unitary matrices $\mathbf{U}$ and $\mathbf{V}$ iteratively by decomposing the reconstruction result of equation (2) as a new prior image data, which is usually a better estimate of the object image. Figure 3 shows a flowchart of the algorithm.

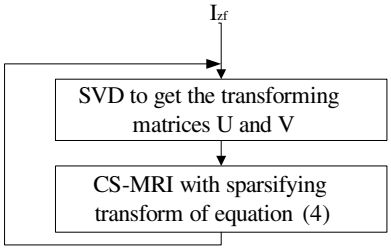


**Figure 3.** Flowchart of the proposed algorithm.

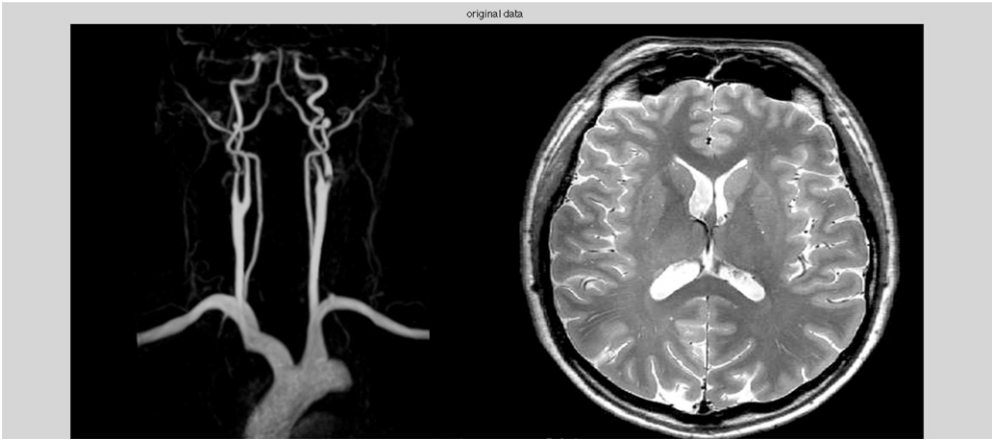


**Figure 4.** The target images.

*MR object images*

As shown in figure 4, to compare the commonly used sparsifying transforms in the CS-MRI with the proposed one, a brain image and an angiogram were used to test the reconstruction performance. The MR brain image, as a complex form with more contrast in pixel domain, can be employed to test the performance of the method on general MR images. The MR angiogram can be used to represent MR images already sparse in the pixel domain. All images were 512 by 512 pixels. Four aspects of the different sparsifying transforms were evaluated: (i) the peak SNR (PSNR) for quality of the reconstructed image, (ii) the image reconstruction time, (iii) the sparsity and (iv) the data fidelity to the measurement. The PSNR is calculated by

$$\mathrm{PSNR} = 10 \log_{10} \frac{1}{\mathrm{MSE}} \tag{5}$$

where MSE is the mean squared error between target and the reconstructed images.

*K-space sampling scheme*

*K*-space was randomly undersampled along the phase direction as shown in figure 5. The random sampling with a Gaussian density distribution in the sensing matrix was validated to provide incoherence with a sparsity basis in compressed sensing. The central region of

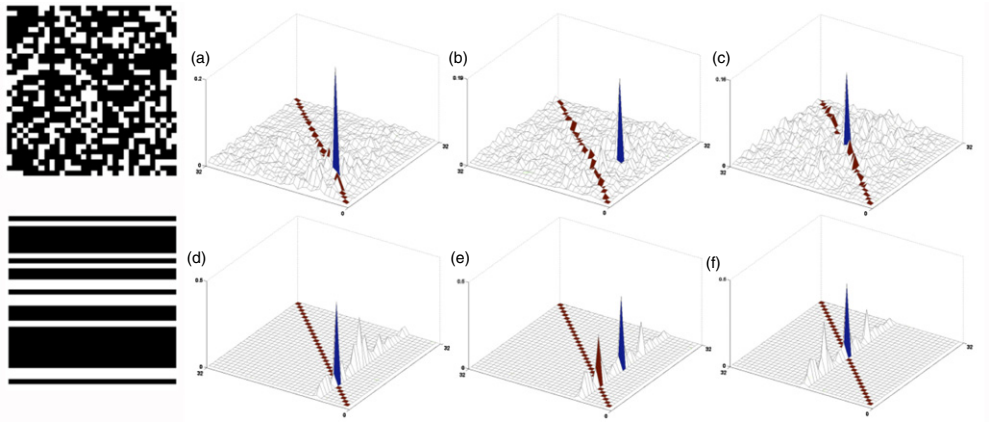


**Figure 5.** The TPSF of the proposed transform for different under-sampling patterns (row) and different positions of the unit pulse (column). The top is the TPSF by 2D *k*-space random sampling, and the bottom is the TSPF by 1D (phase encoding only) *k*-space random sampling.

*k*-space was fully sampled, which contains the major low frequency information. The 2D random undersampling scheme was also implemented to study the incoherence between the sensing matrix and proposed sparsity basis. By adjusting the density function, we randomly sampled 110 lines, 140 lines, 170 lines, 200 lines, 230 lines, and 260 lines of the full *k*-space data respectively to test the CS-MRI performances. It is expected that even with fewer samples, the randomly undersampled *k*-space should contain sufficient information of the target MR image.

*Algorithms for CS reconstruction*

Equation (2) is a constrained convex optimization problem. In this work, the constrained convex optimization problem in equation (2) was solved by considering its Lagrangian form described as follows:

$$\text{Minimize}: \quad f(m) = \|\varphi_F(m) - y\|_2 + \lambda\|\psi(m)\|_1. \tag{6}$$

The nonlinear conjugate gradient (NLCG) with a total variation (TV) regularization (Rudin *et al* 1992, Lustig *et al* 2007) was applied to solve the unconstrained problem as described in equations (4) and (6). As shown in table 1, two stop criteria were set: one was the *Gradmag*, which is the gradient magnitude of $f(m)$; the other was *MaxIter*, which is the maximum number of iterations for NLCG. When it meets either of the two stop criteria, the reconstruction will stop. To fairly compare the reconstruction performance of the various transforms, we set the $Gradmag = 1 \times 10^{-30}$ and the $MaxIter = 8$ for each sparsifying transform. According to the simulation, the image reconstruction can be stabilized and reach the best quality after two or three iterations. So, the number of iterations for updating the sparsifying transform was set to 4. The algorithm was implemented in Matlab (Release 2010a). All simulations were performed on a MacBook Pro with a 2.4 GHz Intel Core 2 Duo processor and a 4 GB memory.

**Table 1.** Outline of the reconstruction for the CS-MRI framework.

**Inputs:**
**y**: under-sampled $k$-space measurements;
$\mathbf{I}_{zf}$: initial image by applying inverse Fourier transform directly to the under-sampled $k$-space;
$\varphi_F$: under-sampling Fourier sensing operator;
$\boldsymbol{\Psi}$: proposed sparsifying transform;
$\boldsymbol{\lambda}$: a positive constant between 0 and 1 (0.03 in this work);
*GradMag*: stopping criteria by gradient magnitude ($1 \times 10^{-30}$ in this work);
*MaxIter*: stopping criteria by the max number of iterations (8 in this work);
$\boldsymbol{n}$: number of iterations for updating the proposed sparsity basis (4 in this work);
$\alpha$, $\beta$: line search parameters ($\alpha = 0.05$, $\beta = 0.6$ in this work).

**Output**:
$m$: the reconstruction result.

% Initialization
$k = 0$; $m = 0$; $m_0 = \mathbf{I}_{zf}$; $g_0 = \nabla f(m_0)$;$\Delta m_0 = -g_0$;
$[\mathbf{U}, \mathbf{S}, \mathbf{V}] = \text{SVD}(m_0)$; % generate the sparsifying transform using the prior image data
% **Iterations to update the sparsifying transform basis**
for $i = 1{:}n$
  % **Iterations in NLCG algorithm**
  while($\|g_k\|_2 >$ *GradMag* and $k <$ *MaxIter*){
    $t = 1$; while $(f(m_k + t\Delta m_k) > f(m_k) + \alpha t \bullet \text{real}(g_k^* \Delta m_k))$ $\{t = \beta t\}$
    $m_{k+1} = m_k + t\Delta m_k$;
    $g_{k+1} = \nabla f(m_{k+1})$;
    $\gamma = \frac{\|g_{k+1}\|_2^2}{\|g_k\|_2^2}$;
    $\Delta m_{k+1} = -g_{k+1} + \gamma \Delta m_k$;
    $k = k + 1$;}% **finish the iterations in NLCG algorithm**
  $k = 0$; $m = 0$; $m_0 = m_k$; $g_0 = \nabla f(m_0)$;$\Delta m_0 = -g_0$;% update the image $m_0$ by using the previous reconstruction $m_k$
  $[\mathbf{U}, \mathbf{S}, \mathbf{V}] = \text{SVD}\ (m_0)$;% update the sparsifying transform using the new image.
end% **finish the iterations to update the sparsity basis**.

## Results and discussion

### *Test of incoherence*

The incoherence between the sparsity basis and the sensing matrix is one of the fundamental criteria for applying compressed sensing. Mathematically, it is not straightforward to test the incoherence. In this case, we adopt the transform point spread function (TPSF) (Lustig *et al* 2007) to evaluate the incoherence between the proposed sparsity basis and the Fourier sensing matrix. Figure 5 shows the TPSF of the SVD sparsity basis for different undersampling patterns (rows) with different position of the unit pulse (columns). The **U** and **V** matrices were retrieved from the MR brain image. Though the SVD sparsity basis is data-adaptive, the incoherence characteristics were observed to remain consistent with different types of MR image. The top row (a–c) illustrates the TSPF by 2D $k$-space random sampling with a red unit pulse located at the dominant diagonal, the off-diagonal and the minor diagonal, respectively. The bottom row (d–f) illustrates the TPSF by 1D (phase encoding only) $k$-space

**Table 2.** Comparison of the computing time (in seconds).

| Line | 110 | 140 | 170 | 200 | 230 | 260 |
|---|---|---|---|---|---|---|
| Brain | | | | | | |
| SVD | *161.5001* | *158.8007* | *171.7865* | *167.5317* | *172.9755* | *156.9833* |
| DWT | 300.8306 | 301.9727 | 299.9399 | 302.3034 | 306.6273 | 303.5215 |
| DCT | 216.4052 | 217.2460 | 216.9223 | 220.8161 | 225.7825 | 221.4718 |
| Angiogram | | | | | | |
| SVD | 152.4741 | 159.4969 | 164.9503 | 156.1093 | 154.4704 | 192.7666 |
| DWT | 305.1093 | 318.3699 | 309.2712 | 392.6533 | 304.3757 | 306.3913 |
| IDT | *52.2626* | *59.0000* | *56.4745* | *51.7941* | *57.5396* | *53.6698* |

random sampling with a red unit pulse located at the dominant diagonal, off-diagonal and minor diagonal, respectively. The TSPF behavior reveals that the 2D undersampling in the *k*-space can enhance the incoherence between the sparsity basis and the sensing matrix by suppressing the interference from the unit pulses to other components. In the pixel domain, the reconstructed image with this sampling method has fewer artifacts and thus a better image quality. On the other hand, we noted that the dominant components on the matrix diagonal have a better TPSF than other unit pulse locations. In other words, because the major image information is compressed on the dominant diagonal components, the proposed method can naturally reduce the weight of the interference from the minor components in the sparsity basis. This is not the case in other sparsity bases where the TPSF is more evenly distributed.

### *The brain image*

The brain image was obtained by scanning a healthy male volunteer's brain with a Bruker 2T whole-body MRI system. The brain image is not sufficiently sparse in the pixel domain. As commonly used sparsity bases in this case, the DWT and DCT were implemented to compare the reconstruction performance on the brain image with the proposed method. Table 2 shows that with different reduction factors, the proposed method outperformed the DWT- and DCT-based methods on computing efficiency. The computing time of the proposed method was nearly half of DWT. Table 3 and figures 6–8 illustrate that with different reduction factors, the three methods adopted in this work achieved quite close image qualities. Based on table 3, it is shown that the proposed method still provides slightly higher PSNR among others. For sparsity, the proposed transform generates more and more sparse coefficients with the iterations and exhibits better sparsity than DCT and DWT, as shown in figures 9 and 10. The fidelity of the reconstruction to the measured data is calculated and collected into table 4. The proposed method presented the best data fidelity. In view of the comparisons above, it can be safely concluded that for MR images which have a complex form and considerable contrast in pixel domain, the proposed method can provide very good reconstruction performance. These results indicate the potential of this method for CS-MRI with heavy computing scenarios, such as dynamic MRI.

### *The angiogram*

The reconstruction performance of CS-MRI with sparsity bases was also tested on a MR angiogram. The angiogram is already known to be sparse in the pixel domain naturally,

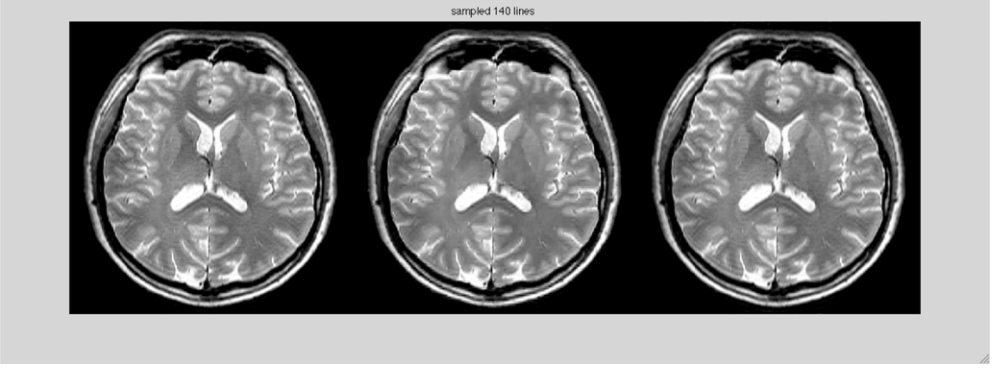


**Figure 6.** The results of the brain image with 140 lines sampled. From left to right, the sparsifying transforms applied are SVD, DWT and DCT.

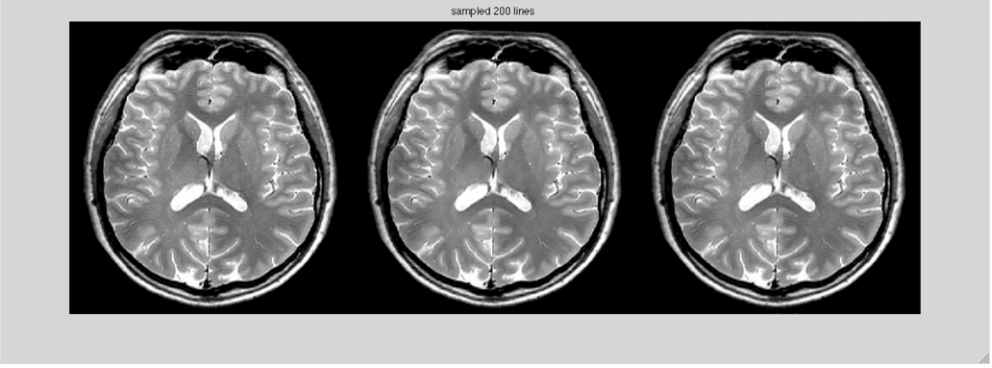


**Figure 7.** The results of the brain image with 200 lines sampled. From left to right, the sparsifying transforms applied are SVD, DWT and DCT.

**Table 3.** Comparison of the image quality in terms of PSNR (db).

| Line | 110 | 140 | 170 | 200 | 230 | 260 |
|---|---|---|---|---|---|---|
| Brain | | | | | | |
| SVD | *+25.82* | *+27.73* | *+29.60* | *+31.49* | *+32.94* | *+35.12* |
| DWT | +25.55 | +27.28 | +29.18 | +30.97 | +32.32 | +33.96 |
| DCT | +25.02 | +27.10 | +28.90 | +30.45 | +31.67 | +33.35 |
| Angiogram | | | | | | |
| SVD | *+37.90* | *+41.47* | *+44.88* | *+48.38* | *+50.37* | *+51.96* |
| DWT | +37.26 | +39.42 | +41.36 | +42.89 | +43.75 | +44.48 |
| IDT | +35.49 | +35.93 | +36.21 | +36.34 | +36.38 | +36.41 |

compared to brain images. The MR angiogram was obtained using a Siemens MAGNETOM Avanto 1.5T system. The IDT was commonly used for this type of images as the sparsity basis in many previous studies. IDT, DWT and SVD bases were applied in this case to compare the reconstruction performance.

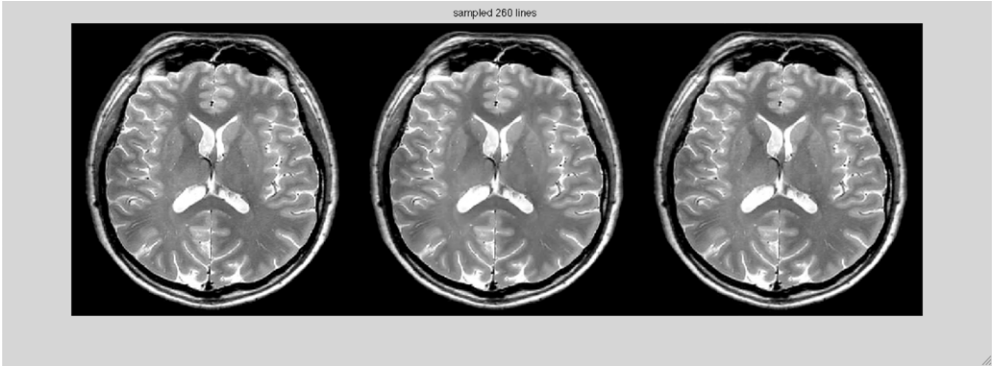


**Figure 8.** The results of the brain image with 260 lines sampled. From left to right, the sparsifying transforms applied are SVD, DWT and DCT.

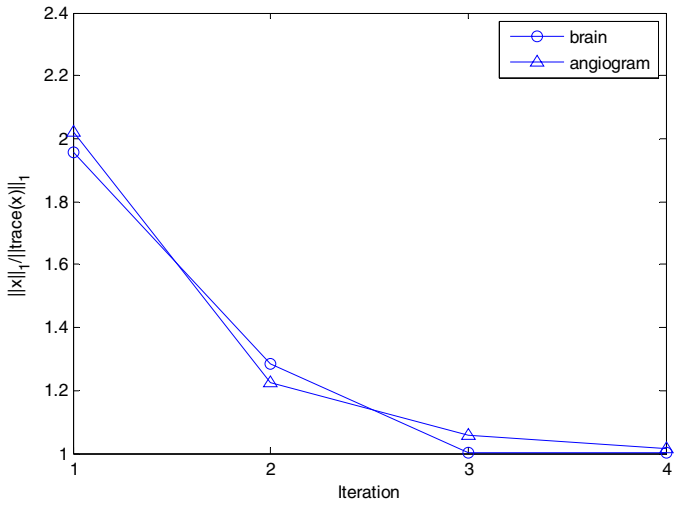


**Figure 9.** The ratio $\|x\|_1 / \|\text{trace}(x)\|_1$ of the proposed method for brain and angiogram images will converge to 1 with the iterations. That is, the diagonal coefficients after proposed transformation will be more and more dominant with the iterations.

As shown in table 2, the IDT on the MR angiogram performed the most efficient computations requiring about 1/6 of the computation time of the DWT. Table 3 and figures 11–13 demonstrate that the image qualities from the three methods were quite close to each other, with the proposed method slightly outperforming the others on PSNR. For sparsity, the proposed method provides similar results with that of brain image and shows better sparsity than DWT and IDT as shown in figures 9 and 14. As shown in table 4, the proposed method achieved the best data fidelity, with a factor of over 10 times improvement over the IDT.

It seems then that, for MR angiograms, the IDT provides the most efficient computing solution. However, the proposed method achieves better image quality, and improved data fidelity. Thus, premier reconstruction quality with the proposed method is still preferable in the case with object images already sparse in the pixel domain.

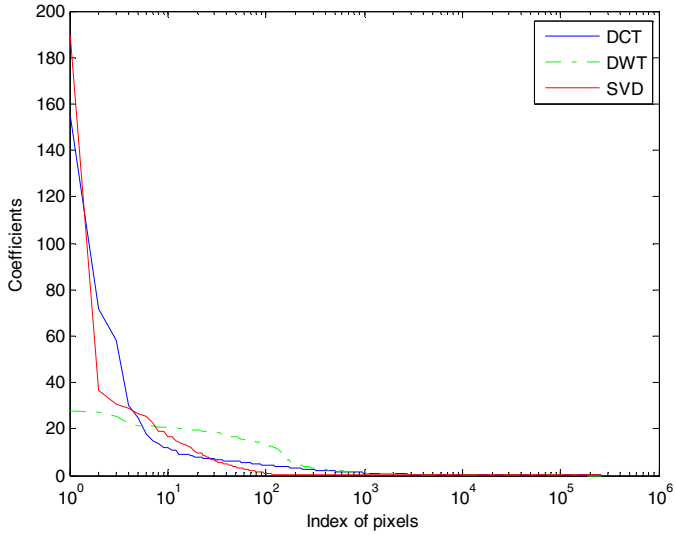


**Figure 10.** Comparison of the sparsity of SVD, DWT and DCT for brain image. The abscissa is the index of the pixels, and the ordinate is sorted coefficients after sparsifying transformation.

**Table 4.** Comparison of the data fidelity by $\|\varphi_F(m) - y\|_2$.

| Line | 110 | 140 | 170 | 200 | 230 | 260 |
|---|---|---|---|---|---|---|
| Brain | | | | | | |
| SVD | *1.32* | *1.33* | *1.47* | *1.49* | *1.58* | *1.38* |
| DWT | 4.22 | 4.25 | 4.30 | 4.38 | 4.59 | 4.70 |
| DCT | 3.48 | 3.66 | 3.95 | 4.20 | 4.50 | 4.68 |
| Angiogram | | | | | | |
| SVD | *0.64* | *0.62* | *0.66* | *0.64* | *0.67* | *0.71* |
| DWT | 2.28 | 2.25 | 2.35 | 2.40 | 2.42 | 2.47 |
| IDT | 7.66 | 7.66 | 7.68 | 7.69 | 7.69 | 7.69 |

The reconstruction performance over different reduction factors is also a criterion to investigate the practicability of applying the CS-MRI methods. Table 2–4 and figures 6–14 demonstrate various characteristics of the proposed method and other sparsity bases, including DCT, DWT and IDT, with the aforementioned *k*-space undersampling schemes.

With the same stopping criteria configured in the NLCG solver, all the methods illustrate consistent performance on computing time and data fidelity. The PSNR was observed to increase with increasing *k*-space measurements as expected.

The analysis of the proposed method and comparison with other existing sparsity bases has shown its advantages as a data-adaptive sparsity basis for CS-MRI framework. The case studies using this method with typical MR object images illustrate its efficient computing performance and better reconstruction quality over the predefined sparsity bases in the CS-MRI framework. Future work with this method may involve dynamic MRI, which requires heavy computation with adaptive sparsity basis in demand.

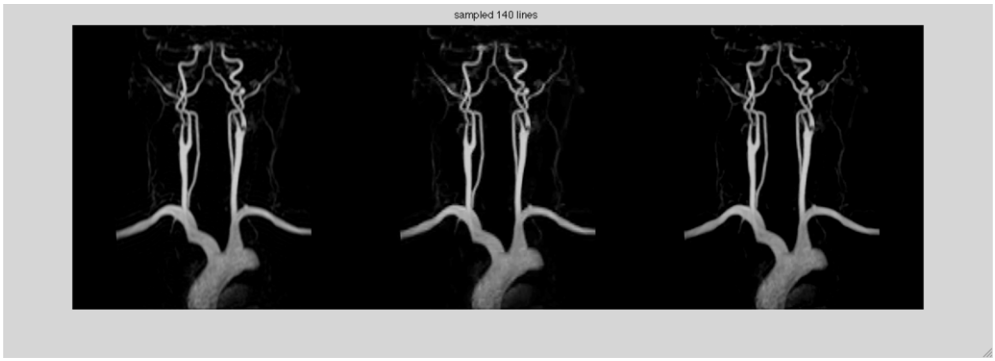


**Figure 11.** The results of the angiogram with 140 lines sampled. From left to right, the sparsifying transforms applied are SVD, DWT and IDT.


**Figure 12.** The results of the angiogram with 200 lines sampled. From left to right, the sparsifying transforms applied are SVD, DWT and IDT.


**Figure 13.** The results of the angiogram with 260 lines sampled. From left to right, the sparsifying transforms applied are SVD, DWT and IDT.

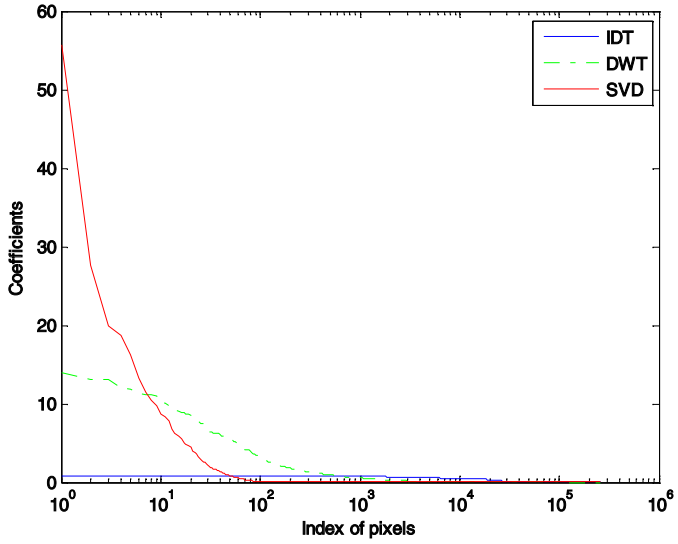


**Figure 14.** Comparison of the sparsity of SVD, DWT and DCT for angiogram image. The abscissa is the index of the pixels, and the ordinate is sorted coefficients after sparsifying transformation.

## Conclusion

This paper proposed a method to construct the data-adaptive sparsity basis for the CS-MRI framework. The computational efficiency and image quality with this method were demonstrated with two typical types of MR image. Comparison against conventional sparsity bases illustrated that the proposed method is capable of accelerating the computing process, while still achieving accurate image reconstruction. As a simple and efficient improvement in the CS-MRI framework, the proposed method may find good application in speed-sensitive CS-MRI applications with heavy computations, such as cardiac dynamic MRI.

## References

Ahmed N, Natarajan T and Rao K R 1974 Discrete cosine transfom *IEEE Trans. Comput.* **23** 90–3

Bilgin A, Kim Y, Liu F and Nadar M S 2010 Dictionary design for compressed sensing MRI *Proc. of 2010 Meeting of the International Society for Magnetic Resonance in Medicine (Stockholm, Sweden)*

Candes E, Romberg J and Tao T 2006 Stable signal recovery from incomplete and inaccurate measurements *Commun. Pure Appl. Math.* **59** 1207–23

Donoho D 2006 Compressed sensing *IEEE Trans. Inf. Theory* **52** 1289–306

Griswold M A, Jakob P M, Heidemann R M, Nittka M, Jellus V, Wang J, Kiefer B and Haase A 2002 Generalized autocalibrating partially parallel acquisitions (GRAPPA) *Magn. Reson. Med.* **47** 1202–10

Griswold M A, Jakob P M, Nittka M, Goldfarb J W and Haase A 2000 Partially parallel imaging with localized sensitivities (PILS) *Magn. Reson. Med.* **44** 602–9

Jolliffe I T 2002 *Principal Component Analysis* 2nd edn (New York: Springer)

Larkman D J and Nunes R G 2007 Parallel magnetic resonance imaging *Phys. Med. Biol.* **52** R15–55

Liang D, Liu B, Wang J and Ying L 2009 Accelerating SENSE using compressed sensing *Magn. Reson. Med.* **62** 1574–84

Lustig M, Donoho D and Pauly J M 2007 Sparse MRI: the application of compressed sensing for rapid MR imaging *Magn. Reson. Med.* **58** 1182–95

Mallat S G 1999 *A Wavelet Tour of Signal Processing* 2nd edn (New York: Academic Press)

Otazo R, Kim D, Axel L and Sodickson D K 2010 Combination of compressed sensing and parallel imaging for highly accelerated first-pass cardiac perfusion MRI *Magn. Reson. Med.* **64** 767–76

Pruessmann K P, Weiger M, Scheidegger M B and Boesiger P 1999 SENSE: sensitivity encoding for fast MRI *Magn. Reson. Med.* **42** 952–62

Rubinstein R, Bruckstein A M and Elad M 2010 Dictionaries for sparse representation modeling *Proc. IEEE* **98** 1045–57

Rudin L I, Osher S and Fatemi E 1992 Nonlinear total variation based noise removal algorithms *Phys.* D **60** 259–68

Sodickson D K and Manning W J 1997 Simultaneous acquisition of spatial harmonics (SMASH): fast imaging with radiofrequency coil arrays *Magn. Reson. Med.* **38** 591–603

Westbrook C, Roth C K and Talbot J 2005 *MRI in Practice* 3rd edn (New York: Wiley-Blackwell)

Yang J, Zhang D, Frangi A F and Yang J 2004 Two-dimensional PCA: a new approach to appearance-based face representation and recognition *IEEE Trans. Pattern Anal. Mach. Intell.* **26** 131–7